Revision 3

Pressure induced structural transformations in the low cristobalite form of $AlPO_4$

H. K. Poswal[1], Nandini Garg[1], Maddury Somayazulu[2] and Surinder M. Sharma[1]

[1]High Pressure and Synchrotron Radiation Physics Division, Bhabha Atomic Research Centre, Mumbai 400085, India

[2]Geophysical Laboratory, Carnegie Institution of Washington, Washington DC, USA

Abstract

We have investigated the high pressure behavior of low cristobalite form of $AlPO_4$ (c-$AlPO_4$) using a combination of Raman scattering, synchrotron powder x-ray diffraction and classical molecular dynamics simulations. Our experiments indicate that under non-hydrostatic conditions c-$AlPO_4$ initially transforms to a monoclinic phase, which then transforms to the Cmcm phase via an intermediate, disordered structure. In contrast, x-ray diffraction measurements made under hydrostatic conditions show that the ambient structure transforms directly to the Cmcm phase. Our classical molecular dynamics simulations, carried out under hydrostatic conditions, also show that c-$AlPO_4$ directly transforms to the Cmcm phase at ~13 GPa.

Keywords: Cristobalite, high pressure, Raman scattering, synchrotron x-ray diffraction, classical molecular dynamics, $AlPO_4$

Introduction

$AlPO_4$ and $GaPO_4$ are iso-electronic analogs of silica and hence are iso-structural to silica polymorphs. Due to this, polymorphs of these phosphates have several properties similar to the silica polymorphs and hence have been studied to understand a number of geophysically relevant phenomena. In fact high pressure studies on $AlPO_4$ in the quartz form created a lot of excitement because of the claims of a memory glass effect, which was however, disproved subsequently (Kruger and Jeanloz, 1990; Sharma et al., 2000).

Apart from its geophysical importance, c-$AlPO_4$ is extensively used in industry due to its excellent properties like high melting point, low Young's modulus, low oxygen permeability and good erosion resistance (Huang et al., 2010; Morris et al., 1977). For example it is an integral part of hardened alumino phosphate cements (Bakunov and Shayakhmetov, 2007) and has been used as a binder for mullite silica fibres which are used as insulators in thermal power plants (Pitak and Churilova, 2004). It has recently been used as a protective coating on C-C composites which are used in aircraft and aerospace industries (Huang et al., 2010). Since the property of materials significantly depends on their structure, and the usability of materials in industry is limited by their

phase stability, it is important to investigate the structural stability of c-$AlPO_4$. There have been extensive theoretical and experimental studies on silica and its polymorphs, however, phosphates of aluminium and gallium have been relatively less explored, in particular in the low cristobalite form.

Experiments on α−cristobalite SiO_2 (c-SiO_2) have shown that, depending upon the degree of hydrostaticity of the applied pressure, it may amorphize or undergo several symmetry lowering crystal to crystal phase transitions (Gratz et al., 1993; Palmer and Finger, 1994; Palmer et al., 1994; Tsuchida and Yagi, 1989). These results were validated by classical molecular dynamics (MD) simulations where Garg and Sharma (2007) showed that c-SiO_2 becomes disordered when simulated at P,T conditions representative of shock Hugoniot and Liang et al., (2007) showed that under non-hydrostatic conditions the transition pathways and the high pressure phases are very sensitive to the presence of anisotropic stresses. MD calculations of several authors indicate that the inter-atomic potentials and the number of unit cells used for the simulation constrain whether c-SiO_2 transforms directly to six coordinated stishovite or via an orthorhombic Cmcm phase (Dove et al., 2000a; Dove et al., 2000b; Keskar and Chelikowsky, 1992; Tse and Klug, 1991; Tsuneyuki et al., 1989; Tsuneyuki et al., 1988). Though Klug and Tse (ab-initio studies) did observe that a lattice distortion precedes the c-SiO_2 to stishovite transformation (Klug et al., 2001), subsequent theoretical calculations (both ab-initio and MD) of Huang et al. did not support the formation of the Cmcm phase at high pressure. They have shown that the first high pressure phase of cristobalite silica has an orthorhombic structure (S. G. : $C222_1$) (Huang et al., 2006).

In contrast to c-SiO_2, one of the early studies on cristobalite phosphates showed that $GaPO_4$ transforms directly to the orthorhombic Cmcm phase at ~ 16.5 GPa whereas c-$AlPO_4$ amorphizes (Robeson et al., 1994). These authors had attributed amorphization in c-$AlPO_4$ to the large Al-O-P angle. Subsequent MD simulations (Murashov et al., 1995) on c-$GaPO_4$ were in qualitative agreement with the experimental results. The discrepancy in the transformation pressures was attributed to the non directional nature of the pair potentials. However, recent experiments (Chio et al., 2008; Ming et al., 2007) on c-$GaPO_4$ indicate that its high pressure behavior is somewhat similar to that of c-SiO_2 though the monoclinic structures of the high pressure phases are different. Both x-ray diffraction (XRD) and Raman spectroscopic studies show that c-$GaPO_4$ undergoes either one or two phase transformations to a monoclinic phase prior to the transformation to the Cmcm phase.

Unlike c-SiO_2, so far none of these studies have shown that the Cmcm phase of $GaPO_4$ further transforms to a stishovite phase. Since all the cations in stishovite are six coordinated it is possible that the high stability of the PO_4 tetrahedra (due to the strong P-O covalent bond) inhibits the formation of the denser phases like stishovite or post stishovite. Recent studies (Pellicer-Porres et al., 2007) on quartz structured α-$AlPO_4$ have however, shown that when it is pressurized to > 46 GPa the Cmcm phase transforms to a monoclinic $CaCl_2$ type of phase where the phosphorous atoms

are six coordinated. Thus in these APO_4 (A : Al, Ga etc.) compounds the Cmcm phase may be thought of as an intermediate phase, between four-fold and six-fold structures, stabilized by the resistance to the breaking of the strong PO_4 bonds. Hence it is possible that if pressurized to sufficiently high pressures $GaPO_4$ may also transform to a denser phase similar to c-SiO_2.

Since the quartz forms of $AlPO_4$ and $GaPO_4$ show similar phase transitions at high pressure, it is surprising that c-$AlPO_4$ should amorphize instead of undergoing crystal to crystal phase transitions. It is possible that like c-SiO_2 the high pressure behavior of the other APO_4 compounds may also be sensitive to the hydrostaticity of the pressure transmitting medium. Hence for a consistent understanding of these iso-electronic, iso-structural compounds it is necessary to do a careful investigation on the high pressure behavior of c-$AlPO_4$. We have therefore studied the high pressure behavior of this compound employing x-ray diffraction, Raman scattering and MD simulations.

Methodology:

Experimental Details

The orthorhombic low-cristobalite form of $AlPO_4$ was prepared by co-precipitation followed by high temperature annealing of the precipitate. Amorphous precipitate of $AlPO_4$ was prepared by adding NH_4OH to an aqueous solution of aluminum chloride and H_3PO_4. The precipitate was dried at about 175°C and was then annealed at 1300°C for about 24 hrs. The sample was well ground and was characterized with the help of x-ray diffraction and Raman spectroscopy. The lattice constants of c-$AlPO_4$ were found to be a=7.0673(6) Å, b=7.0763(6) Å, c=6.9751(3) Å in agreement with earlier published data (Achary et al., 2003).

High pressure x-ray diffraction experiments were carried out on beamline 16ID-B of HPCAT at the Advanced Photon Source using a diamond anvil cell (DAC). c-$AlPO_4$ powder and a tiny chip of ruby were loaded in a gasket hole (with diameter ~ 0.2 mm) drilled in a pre-indented rhenium foil. Two sets of experiments were carried out on c-$AlPO_4$ upto 11.3 and 43 GPa using x-ray wavelength of 0.4028 Å and 0.4298 Å respectively. In the first experiment silicone oil was the pressure transmitting medium (PTM) whereas in the second experiment, nitrogen was used as the PTM. In both these experiments, pressure inside the sample chamber was monitored by the ruby fluorescence line shift (Mao et al., 1986). The diffraction data which was collected using an image plate detector was converted into one dimensional diffraction profiles with the help of FIT2D software (Hammersley et al., 1996).

Raman measurements were carried out using a 460 mm single stage double pass monochromator coupled to a liquid N_2 cooled CCD detector. The Raman scattering was measured using the 488 nm or the 514.5 nm lines of an Ar ion laser as a light source and a supernotch filter was used to cut off the Rayleigh scattered light. The size of the laser spot in these micro Raman

experiments was < 5 μm. The powder sample was loaded in a diamond anvil cell along with a tiny chip of ruby for pressure calibration. Typical relative error in measurement of pressure in hydrostatic environment using our system is about 0.01 GPa. Since the sample was found to interact with methanol-ethanol mixture, experiments were carried out using either Argon, silicone oil or without any PTM.

Computational Details

Molecular dynamics simulations were carried out using a modified Nose-Hoover algorithm (N, P, T) as implemented in the DL_POLY (Smith et al., 2003). The equations of motion were integrated every 2.0 fs using the Verlet leapfrog algorithm. Initial macro cell was generated by applying the translation symmetry on the experimentally determined structure of c-$AlPO_4$ in the space group $C222_1$. The macro cell contains (6x6x4) unit cells with 3456 atoms (576 Al + 576 P + 2304 O). The simulations were carried out at 300 K upto the maximum pressure of 160 GPa, (with ΔP = 2 GPa) employing semi empirical pair potentials of van Beest et al. (1990). We should also note that these pair potentials have been earlier used to understand the high pressure behavior of berlinite and have been able to stabilize the Cmcm phase at high pressures. Ramaniah et al. (2003) have shown that the results obtained from both MD and ab-initio calculations of α-quartz form of $AlPO_4$ were close, indicating that these pair potentials could capture the main physics of both the α-quartz and Cmcm phases of $AlPO_4$. These potentials are also known to simulate the different polymorphs of the $AlPO_4$ phase (van Beest et al., 1990) and therefore we feel that they are good enough to understand the high pressure behavior of cristobalite $AlPO_4$. In the present calculations the system was considered as equilibrated when the fluctuations in the macroscopic parameters like total energy, cell volume etc. were ~ 0.001%. The system was equilibrated at most of the pressures for 100 ps but close to the transition pressures it was allowed to equilibrate for much longer time of 300 ps. The equilibrium properties were calculated by averaging over 2000 time steps.

Results and Discussion:

Experimental

The low temperature phase of c-$AlPO_4$ crystallizes in the orthorhombic space group $C222_1$ (D_2^5) with four formula units per unit cell. (The primitive cell contains two formula units.) Here it is worth mentioning that the space group of the first high pressure phase of c-SiO_2 has also been determined to be $C222_1$ (Liang et al., 2007). According to the factor group analysis, the symmetry classification of all the 36 modes is (Rokita et al., 2000) $\Gamma_{AlPO4}=8A+10B_1+9B_2+9B_3$ with acoustic modes belonging to $B_1+B_2+B_3$. All the A-modes are Raman active, whereas only B_1, B_2 and B_3 are

IR active. At ambient conditions, internal and external modes observed by us are in good agreement with earlier reported values (Nicola et al., 1978; Rokita et al., 2000). Raman spectrum of c-$AlPO_4$ with silicone oil as PTM shows higher background and hence poorer signal to noise ratio than without any PTM. Though recently Argon has been shown to be quasi hydrostatic till ~ 10 GPa (Klotz et al., 2009) our results obtained with Ar or without any PTM were found to be similar. This similarity of the results may be arising from non-hydrostatic environment caused by overfilling of the sample in the gasket, even when Argon was used as a PTM. This was necessary due to inherent weak Raman signal of the sample.

Figure 1 shows the Raman spectra recorded without PTM at a few representative pressures. At ambient conditions, consistent with the results of Rokita et al. (2000), the lattice vibration mode was observed at 278 (P1) cm^{-1} and a doublet of two overlapping modes (corresponding to the two dimensional (2D) bending modes of $[PO_4]^{3-}$ tetrahedra) were observed at ~ 380 (P2) cm^{-1} and 390 (P3) cm^{-1}. The mode at ~ 482 (P4) cm^{-1} can be assigned to the 3-dimensional bending mode of $[PO_4]^{3-}$ tetrahedra. The intense vibrational mode observed at 1119 (P6) cm^{-1} corresponds to the one dimensional symmetric stretch mode of $[PO_4]^{3-}$ tetrahedra and the shoulder at ~ 1109 (P5) cm^{-1} may represent the corresponding asymmetric stretch mode. In our high pressure DAC experiments the intensity of the aluminum sub-lattice band at 566-735 cm^{-1} was found to be quite weak.

With increase in the pressure to ~ 0.4 GPa, Raman modes at 278 (P1) and 1109 (P5) cm^{-1} gained intensity, accompanied by a reduction in the intensity of the low frequency mode (P3) in the doublet of the PO_4 2D bending mode. In addition to this, at ~ 0.6 GPa a new mode was observed at ~ 432 cm^{-1} accompanied with the relative intensity increase of mode P3 compared to mode P2. Emergence of only one mode at ~ 432 cm^{-1} and a weak mode close to mode P1 suggests that these modes might have not been observed (since they were very weak) at ambient conditions but may have gained intensity on the application of pressure. In our ab-initio calculations (Poswal and Sharma) we have seen that this mode exists even at ambient pressure. On further increasing the pressure to ~3.2 GPa most of the modes became broad and weak and merged above 4 GPa (figure 1) to form broad Raman bands centered at ~1100 cm^{-1} and 400 cm^{-1}. These observations seem to suggest tetrahedral distortions, probably indicative of a sluggish first order phase transformation from the ambient orthorhombic structure to another phase (HP-I) . This is supported by the fact that the broad Raman bands evolved into well resolved sharp peaks and gained intensity when further pressurized to ~10.7 GPa. The observation of a larger number of Raman modes in HP-1 (compared to the ambient phase) suggests that the high pressure phase may have a lower symmetry.

On further increase of pressure broadening and diminishing of intensity of the Raman modes is observed above ~ 14.5 GPa. This could be due to the inhomogeneous stress distribution caused by the non-hydrostatic environment, or it could be an indication of a second phase transition to a disordered or poorly crystallized daughter phase. To remove this ambiguity, the sample was

annealed at this pressure by increasing the laser power. This resulted in the appearance of several new broad Raman modes (figure. 1) in the range of 500 to 1200 cm^{-1}. In addition to this, the weak mode observed at ~ 450 cm^{-1} before annealing became sharp after annealing. Even on lowering the laser power these modes were clearly visible. Here it is worth mentioning that this is not an artifact of any reaction between the sample and the PTM as this experiment was carried out without any PTM. The appearance of these new Raman modes shows that the changes in the Raman spectrum at this pressure were essentially due to a phase transformation to a new high pressure phase (HP-II). Robeson et al. (1994) have shown that c-$GaPO_4$ transforms to a $CrVO_4$ type structure at ~16.5 GPa. The comparison of these Raman modes with earlier reported Raman spectrum of $CrVO_4$ type structure (in particular that of $FePO_4$ (Pasternak et al., 1997) and $CuCrO_4$ (Baran, 1994)) suggest that the structure of the second high pressure phase could be similar to the $CrVO_4$ structure (Baran, 1994). These studies are in agreement with our (Poswal and Sharma) ab-initio Plane-Wave Self Consistent-Field (PWSCF) calculations where we observed that c-$AlPO_4$ transforms to the Cmcm structure at high pressure. In that study we did not observe the first monoclinic phase as the calculations were carried out under hydrostatic conditions. These observed phase transitions are clearly visible in the Raman frequency shift versus pressure, as shown in figure 2.

To identify the structures of the different high pressure phases, we will now discuss the results of our x-ray diffraction experiments. Figure 3 shows one dimensional x-ray diffraction patterns of c-$AlPO_4$ at various pressures. The lower two diffraction profiles are from the experiments carried out with silicone oil as a PTM (which remains hydrostatic upto ~2 GPa) and the rest are from the experiments where N_2 was used as a pressure transmitter. The study on these PTM shows that silicone oil remain hydrostatic up to ~ 2 GPa and N_2 up to ~ 10 GPa (Klotz et al., 2009).

The x-ray diffraction pattern at 4.7 GPa (using silicone oil as PTM) shows several new diffraction peaks in comparison with that observed at ambient conditions indicating a phase transition to a lower symmetry phase. This result is consistent with our Raman scattering measurements where we observed that the initial phase is stable below ~ 4 GPa beyond which it transforms. Even in $GaPO_4$ a similar symmetry lowering transition was observed at ~2 GPa. This new high pressure phase (HP1) was indexed using the Crysfire software (Shirley, 2004). Crysfire generated several similar monoclinic solutions with high figure of merit (7.4). These solutions were tested with Le-Bail refinement. The lattice parameters obtained from the best Le-Bail refinement are a= 8.0914(8) Å, b = 4.5432(4) Å, c = 8.838(1) and $\beta = 120.018(9)°$ with goodness of fit parameters Rp = 0.03 and wRp = 0.26. The space group determined from the systematic absences in the diffraction profile was found to be P2. Figure 4 shows the Le-Bail refinement of the experimental data at ~4.7 GPa. Density considerations suggest that this monoclinic phase also has four formula units in each unit cell. To determine whether the structure of this monoclinic phase was similar to any of the known monoclinic polymorphs of silica like Badeyylite etc. we generated these structures

and their respective diffraction patterns, by scaling the volume (the cell constants determined from the Le Bail fit were used) to that of the monoclinic phase observed by us. However, we found that none of the generated diffraction patterns were similar to that of the HP1 phase. Though we could not determine the exact structure of this HP1 phase the ratio of the lattice constants suggest that this phase is distinct from the monoclinic phase observed in c-$GaPO_4$ as well as in c-SiO_2 (Dove et al., 2000b; Ming et al., 2007).

On increasing the pressure beyond 11 GPa the x-ray diffraction pattern showed broad diffraction peaks, indicative of destabilization of the monoclinic structure as also observed in our Raman experiments. In addition to this, when the pressure is fully released from the monoclinic phase, the observed d-values suggest that the compound transforms back to the initial structure, indicating the reversibility of the structural changes. Raman scattering measurements also suggest that it transforms back to the ambient phase.

With Nitrogen as PTM, the diffraction pattern at ~8.1 GPa displayed several new diffraction peaks (figure 3) indicating a phase transformation. This diffraction pattern is distinct from the HP1 diffraction pattern observed in the experiment where silicone oil was used as the PTM. The diffraction pattern of this high pressure phase of c-$AlPO_4$ could be indexed to an orthorhombic structure in the Cmcm space group. This structure was found to be similar to the high pressure phase of c-$GaPO_4$ ($CrVO_4$ type structure) (Robeson et al., 1994). To determine the lattice constants of this phase the diffraction patterns were analysed using the Rietveld refinement method implemented in the GSAS (Larson and Von Dreele, 2000) software. Since nitrogen is used as a PTM all the recorded diffraction patterns were analyzed using two phases ($AlPO_4$ and N_2). Figure 5 shows the Rietveld refined x-ray diffraction pattern at 8.1 GPa with $AlPO_4$ in Cmcm phase and N_2 in δ-phase (Olijnyk, 1990). The lattice parameters obtained from the Rietveld refinement are a= 5.085(1) Å b= 7.360(1) Å and c= 5.838(1) Å (Table 1) with goodness of fit parameters Rp = 0.66 and wRp = 0.18 at 8.1 GPa. The comparison of lattice parameters with the earlier reported values are shown in table 2. The Cmcm phase was found to be stable upto 33.3 GPa as shown in figure 3. The diffraction peaks broadened and diminished in intensity at 41.1 GPa. This could be due to disordering or due to the inhomogeneous distribution of stresses. To reduce the probable non-hydrostatic stresses the sample was annealed to 310ºC at this pressure using external heating (and the pressure measured after annealing was ~ 43.9 GPa). This resulted in sharpening of the diffraction peaks implying the stability of the Cmcm phase upto this pressure.

These x-ray diffraction and Raman scattering measurements show that under non-hydrostatic conditions c-$AlPO_4$ transforms to a monoclinic structure at ~ 4 GPa. This structure becomes unstable above 11 GPa and starts transforming to the Cmcm phase via a disordered phase (which may be due to a thermodynamic barrier affecting the kinetics adversely). However in hydrostatic pressure experiments ambient cristobalite phase directly transforms to the Cmcm phase above 8 GPa. These

observations indicate that, under hydrostatic pressures, cristobalite to Cmcm phase transformation in c-$AlPO_4$ is not kinetically hindered. Even in c-SiO_2 it has been observed that when the simulations were carried out under hydrostatic conditions it transformed to the Cmcm phase (Garg and Sharma, 2007; Tsuneyuki et al., 1989). These simulations also showed that even when c-SiO_2 directly transformed to the stishovite phase it was always via a transient Cmcm phase. However, experiments (Downs and Palmer, 1994; Tsuchida and Yagi, 1989) have shown that if non-hydrostatic stresses are present then c-SiO_2 transforms to a monoclinic phase. This shows that there is a similarity in the high pressure behavior of these APO_4 oxides.

Computational

To understand the atomistic mechanism of phase transitions, we have carried out classical molecular dynamics simulations on c-$AlPO_4$. Cristobalite-$AlPO_4$ was equilibrated at 0.1 MPa and 300 K. The equilibrated final volume determined from these simulations is 328.95 $Å^3$ which compares well with the experimental value 348.83 $Å^3$ i.e., within ~ 6 % . The calculated lattice parameters at this pressure are a = 7.1652 Å, b = 6.9428 Å and c = 6.6125 Å in comparison to the experimentally observed lattice parameters, a = 7.0673(6) Å, b = 7.0763(6) Å, c = 6.9751(3) Å (i.e. within 1.4 %, 1.9% and 5.2 % respectively). This equilibrated structure was subjected to increasing pressure in steps of 2 GPa.

Figure 6 shows the evolution of calculated lattice parameters (calculated are shown by lines and experimental by symbols) of c-$AlPO_4$ with pressure from MD simulations. On increasing pressure the lattice parameter **b** shows less compression compared to **a** and **c**. MD simulations at ~ 13 GPa show a large compression in **a** and **c** lattice parameters accompanied by an abrupt expansion in the **b** parameter, indicating a phase transformation. Evolution of lattice parameters at 13 GPa during MD simulation is given in supplementary information (Figure S1) . These changes result in a volume drop of ~12.4 % at this pressure, confirming it to be a first order phase transition. This phase transformation is at a slightly higher pressure than that found in the experiments. Though the compression trends of calculated and the experimental lattice parameters are same in the Cmcm phase, the calculated lattice parameters are slightly over estimated compared to the experimental ones, as shown in figure 6. Even on release of pressure the Cmcm phase was found to be stable upto ~5 GPa. Below this pressure it transform to a four coordinated phase distinct from the initial phase. This is understandable as c-$AlPO_4$ is a metastable phase at ambient conditions and its formation may depend on the thermodynamic path. For the ambient phase, the bulk modulus and it's derivative obtained by fitting the calculated P-V data to 3rd order Birch Murnghan equation of state gives B_0= 24(3) GPa and B'=6(1) and B_0=29(1) with B' fixed to 4. As we did not have sufficient experimental

data points to determine the bulk modulus of the ambient cristobalite phase, these values could not be compared to the experimental one.

The phase transition displays itself through significant changes in the radial distribution function (RDF) g(r). The RDFs of Al-O , P-O and O-O as a function of pressure is given in supplementary information (Figure S2). At ambient conditions, Al-O RDF shows a sharp peak at 1.74 Å which integrates to 4 implying that Al atoms have four oxygen nearest neighbors having a bond length of ~1.74 Å. However, at ~ 13 GPa this sharp peak splits into two peaks, integrating to 6 implying that at this pressure Al atoms have six nearest neighbors. Analysis of the structure shows that out of the six oxygen atoms coordinated to Al, four are at 1.79 Å and two are at 1.95 Å. These features are similar to that of the Cmcm phase of SiO_2 observed by Tsuneyuki et al. (1989). In contrast to the RDF of Al-O, RDFs of P-O do not show any dramatic changes in the first nearest neighbor peak implying that the PO_4 tetrahedra remain intact up to 160 GPa. In the radial distribution function of O-O there are two well separated peaks, the first peak being more intense and sharp compared to the second one. Both these peaks integrate to 3, indicating that there are 3 first and 3 second nearest neighbors. After the transition, first coordination becomes 4 and second coordination becomes ~9. Structure analysis shows that this is due to the collapse of corner shared tetrahedral network system (cristobalite) to a mixed network of corner shared octahedra and tetrahedra (where individual octahedral are edge shared).

RDF and structural analysis at different pressures suggest that Al becomes six coordinated at 13 GPa while P continues to be four coordinated upto the highest pressure in our simulations. The structure of the high pressure phase was found to be similar to the one observed by Tsuneyuki et al in c-SiO_2 ($CrVO_4$ type) (Tsuneyuki et al., 1988). (Space group of the high pressure structure obtained in the simulation is determined using the FINDSYM software H. T. Stokes, D. M. Hatch, http://stokes.byu.edu/isotropy.html, 2004). It is made of corner linked AlO_6 octahedra and PO_4 tetrahedra. For direct comparison to the x-ray diffraction experiments we generated powder x-ray diffraction patterns from the averaged coordinates at each pressure. At ambient conditions, calculated and experimental diffraction patterns display good agreement in terms of intensity ratios.

At 13 GPa the computed diffraction pattern changed abruptly and it matches well with the diffraction pattern of the 'daughter' phase ($CrVO_4$ type) obtained under hydrostatic conditions. The lattice parameters just across the phase change also compare favorably, viz., **a** = 7.5875 Å **b** = 5.1979 Å and **c** = 5.6688 Å (calculated, 13 GPa) versus **a** = 5.0784(1) Å **b**= 7.3627(1) Å and **c**= 5.8363(1) Å (experimental at ~ 8 GPa) (note that in simulations **a** and **b** axes were interchanged as compared to the experimental setting). These results confirm that the high pressure phase observed in the simulations is the same as observed in our experiments. The new structure i.e. Cmcm ($CrVO_4$ type) is predicted to be stable at least upto 160 GPa in agreement with our experiments where we observed that the Cmcm phase is stable upto ~ 43 GPa (highest pressure achieved in this

experiment). Consistent with our structural analysis presented above, the RDF patterns of released run show that Cmcm phase is stable up to 5 GPa below which it transforms to a four coordinated phase. The calculated bulk modulus and its derivative determined by fitting 3rd order Birch Murnghan equation of state are B_0 = 136(4) GPa and B' = 4.7(2) with V_0 = 240.29(1) Å^3 fairly matching with our experimental values B_0 = 137(5) GPa and B' = 4 (fixed) with V_0 = 230.571(1) Å^3 . Earlier reported bulk modulus and it's derivative are B_0= 118(7) GPa and B' = 4 (fixed) with V_0 = 244.8(6) Å^3 (Pellicer-Porres et al., 2007). The observed discrepancy in our experimental and earlier reported values (Pellicer-Porres et al., 2007) could be due to a better (neon vis-a-vis nitrogen) hydrostatic environment as compared to our studies. It is also possible that since in those studies quartz was transforming to Cmcm and in our study cristobalite was transforming to Cmcm the end product may have a different amount of internal stress or defects which may affect the bulk modulus.

Our MD results show that the cristobalite to Cmcm transition takes place at a higher pressure when compared to the experiments carried out under hydrostatic conditions. In c-$GaPO_4$ the discrepancy in transformation pressures has been attributed to the non-directional nature of the pair potentials. It is possible that even in c-$AlPO_4$ the non-directional nature of the pair potentials may be responsible for the differences in the transformation pressures. However, in the experiments one can not rule out the possibility that even a small amount of non- hydrostaticity may reduce the transformation pressure.

To summarize, our investigations show that the high pressure behavior of c-$AlPO_4$ depends on the degree of hydrostaticity of pressure in the diamond anvil cell. Our Raman scattering and XRD results show that under non-hydrostatic conditions the cristobalite phase first transforms to a monoclinic phase and then to the Cmcm phase, via a disordered state. For this compound the monoclinic and Cmcm phases seem to be separated by a kinetic barrier. However, our XRD and MD simulations show that under hydrostatic pressures the ambient phase transforms directly to the Cmcm phase, a result that is similar to c-SiO_2.

FIGURE CAPTIONS

Figure 1: Raman spectra of c-$AlPO_4$ at a few representative pressures. The presented data are from the high pressure run performed without any pressure transmitting medium. Raman modes of ambient phase are marked by P1, P2, P3, P4, P5 and P6. The mode assignment for Cmcm phase is taken from the ab-initio calculations (Poswal and Sharma, 2011). The mode marked as asterisk does not belong to Cmcm phase and could not be assigned.

Figure 2: Experimentally observed shift of Raman modes of c-$AlPO_4$ with pressure in a non-hydrostatic environment.

Figure 3: Background subtracted x-ray diffraction patterns of c-$AlPO_4$ at a few representative pressures. Lowest two diffraction patterns were recorded with silicone oil as a pressure transmitting medium (λ=0.4028 Å) and the rest of the patterns are recorded with N_2 as pressure transmitter (λ=0.4298 Å). The calculated peak positions of the c-$AlPO_4$ phases at ambient conditions have been indicated by the vertical bars in the figure. The calculated diffraction patterns of N_2 at various pressures are shown in the figure with the red line (Olijnyk, 1990).

Figure 4 Le-Bail refinement of x-ray diffraction pattern at 4.7 GPa (Silicone oil as pressure transmitting medium, λ=0.4028 Å). The experimental data are represented by plus sign, the Le-Bail fit by red line and the difference is denoted by cyan. Vertical bars represent the diffraction peak positions from solid high pressure monoclinic phase of c-$AlPO_4$. The goodness of fit parameters are Rp = 0.03 and wRp = 0.26.

Figure 5 Rietveld refinement of x-ray diffraction pattern at ~8.1 GPa (N_2 as pressure transmitting medium, λ=0.4298 Å) . The experimental data are represented by plus sign, the Rietveld fit by red line and the difference is denoted by cyan. Vertical bars represent the diffraction peak positions from solid N_2 (δ-phase) (Olijnyk, 1990) and high pressure Cmcm phase of c-$AlPO_4$. The goodness of fit parameters are Rp = 0.66 and wRp = 0.18

Figure 6 Evolution of the calculated lattice parameters of **a** (black line), **b** (red line) and **c** (blue line) of the c-$AlPO_4$ phase with pressure as determined from our MD simulations. The experimental lattice parameters at ambient conditions are shown by asterisk symbols and the high pressure lattice parameters **a** (triangle), **b** (square) and **c** (circle) beyond the phase transition are shown as open symbols. Arrows indicate the compression and decompression cycle. The drastic change in the cell constants at ~ 13 GPa indicates the onset of the phase transition in MD.

Table 1. Measured lattice parameters of $AlPO_4$ (cristobalite and Cmcm phase) obtained from Rietveld refinement of diffraction patterns recorded at various pressures with nitrogen as PTM. Lattice parameters in the monoclinic phase (with silicone oil as PTM) are determined using Le-Bail refinements.

Pressure (GPa)	Phase	a (Å)	b (Å)	c (Å)	Beta
0.05	$C222_1$	7.0672(6)	7.0762(7)	6.9752(3)	
4.7	monoclinic	8.0914(8)	4.5431(4)	8.838(1)	120.018(9)
8.1	Cmcm	5.085(1)	7.360(1)	5.838(1)	
12.3	Cmcm	5.065(2)	7.296(3)	5.765(3)	
16.9	Cmcm	5.036(3)	7.220(4)	5.696(3)	
21.4	Cmcm	5.015(2)	7.172(4)	5.667(3)	
26.1	Cmcm	5.009(1)	7.131(2)	5.603(2)	
33.3	Cmcm	4.989(2)	7.023(3)	5.529(2)	
41.1	Cmcm	4.968(2)	6.948(3)	5.463(3)	
43.9*	Cmcm	4.967(2)	6.950(3)	5.441(3)	

* Annealed at 310° C at 41.1 GPa

Table 2. Comparison of lattice parameters in $CrVO_4$ (Cmcm) type structure with earlier reported values.

	P (GPa)	a (Å)	b (Å)	c (Å)	b/a	c/a
*$AlPO_4$	8.1	5.085(1)	7.360(1)	5.838(1)	1.4474	1.1481
†$AlPO_4$	13.9	5.0365(7)	7.2908(9)	5.7491(9)	1.4476	1.1415
‡$GaPO_4$	15.9	5.12	7.31	5.92	1.4277	1.1563
§SiO_2	15	5.20	7.44	5.58	1.4308	1.0731

*(Present study)
†(Pellicer-Porres et al., 2007)
‡(Robeson et al., 1994)
§(Tsuneyuki et al., 1989)

Figure 1

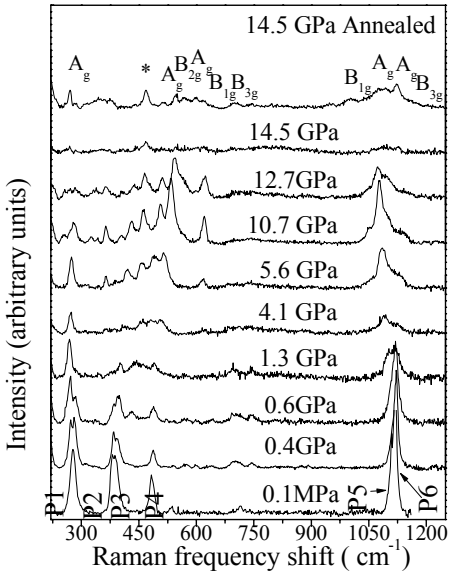

417

418 **Figure 2**

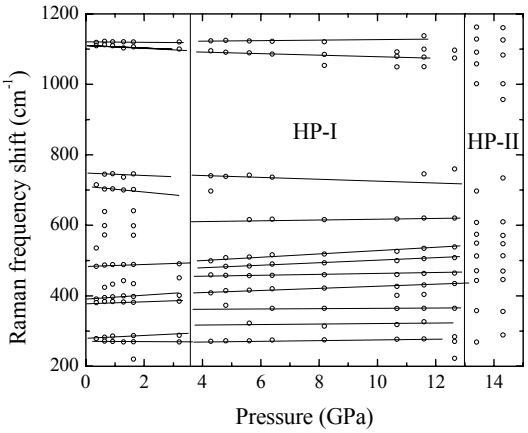

419

420

Figure 3

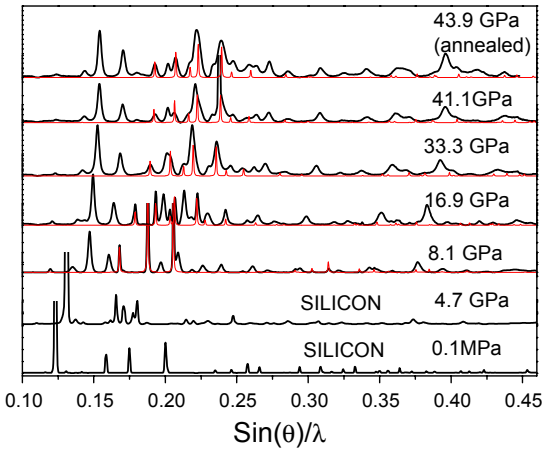

427

428 **Figure 4**

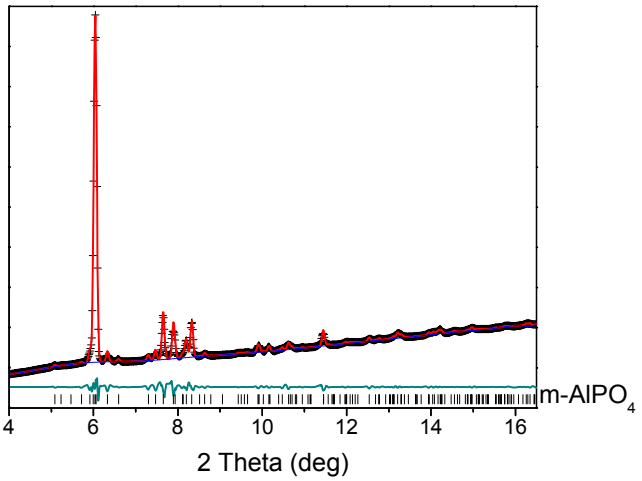

429
430

Figure 5

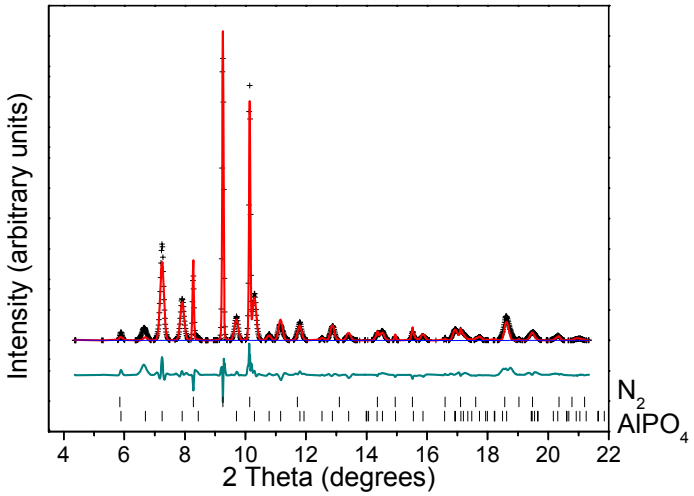

437 **Figure 6**

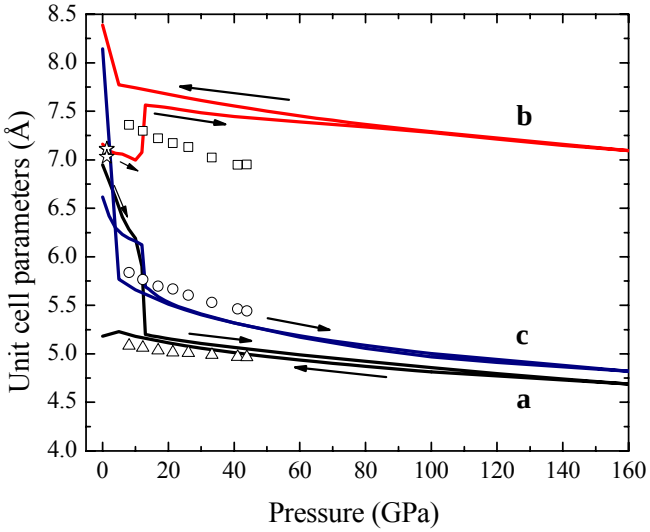

438

439

440

441 References:
442
443
444 Achary, S.N., Jayakumar, O.D., Tyagi, A.K., and Kulshresththa, S.K. (2003) Preparation, phase
445 transition and thermal expansion studies on low-cristobalite type Al1-xGaxPO4 (x=0.0, 0.20,
446 0.50, 0.80 and 1.00). Journal of Solid State Chemistry, 176(1), 37-46.
447 Bakunov, V.S., and Shayakhmetov, U.S. (2007) Deformation of unfired phosphate-bound
448 refractories. Part 3. Deformation of hardened cements on heating and colling. Refractories
449 and Industrial Ceramics, 48, 73-76.
450 Baran, E.J. (1994) Vibrational and Electronic-Spectra of Copper(II) Chromate. Spectrochimica Acta
451 Part a-Molecular and Biomolecular Spectroscopy, 50(14), 2385-2389.
452 Chio, C.H., Sharma, S.K., Ming, L.C., Nakamoto, Y., and Endo, S. (2008) High pressure Raman
453 spectroscopic study of low-cristobalite $GaPO_4$. Journal of Physics: Conference Series, 121,
454 022003.
455 Dove, M., Tucker, M., Redfern, S., Craig, M., Trachenko, K., Marshall, W., and Keen, D. (2000a)
456 High-pressure studies of cristobalite. ISIS annual Report, 32.
457 Dove, M.T., Craig, M.S., Keen, D.A., Marshall, W.G., Redfern, S.A.T., Trachenko, K.O., and
458 Tucker, M.G. (2000b) Crystal structure of the high-pressure monoclinic phase-II of
459 cristobalite, SiO_2. Mineralogical Magazine, 64(3), 569-576.
460 Downs, R.T., and Palmer, D.C. (1994) The Pressure Behavior of Alpha-Cristobalite. American
461 Mineralogist, 79(1-2), 9-14.
462 Garg, N., and Sharma, S.M. (2007) Classical molecular dynamical simulations of high pressure
463 behavior of alpha cristobalite (SiO2). Journal of Physics-Condensed Matter, 19(45), 456201.
464 Gratz, A.J., Deloach, L.D., Clough, T.M., and Nellis, W.J. (1993) Shock Amorphization of
465 Cristobalite. Science, 259(5095), 663-666.
466 Hammersley, A.P., Svensson, S.O., Hanfland, M., Fitch, A.N., and Hausermann, D. (1996) Two-
467 dimensional detector software: From real detector to idealised image or two-theta scan. High
468 Pressure Research, 14(4-6), 235-248.
469 Huang, J.F., Yang, W., and Cao, L. (2010) Preparation of a SiC/Cristobalite-AlPO4 Multi-layer
470 Protective Coating on Carbon/Carbon Composites and Resultant Oxidation Kinetics and
471 Mechanism. J. Mater. Sci. Technol., 26(11), 1021-1026.
472 Huang, L., Durandurdu, M., and Kieffer, J. (2006) Transformation pathways of silica under high
473 pressure. Nature Materials, 5(12), 977-981.
474 Keskar, N.R., and Chelikowsky, J.R. (1992) Structural-Properties of 9 Silica Polymorphs. Physical
475 Review B, 46(1), 1-13.
476 Klotz, S., Chervin, J.C., Munsch, P., and Le Marchand, G. (2009) Hydrostatic limits of 11 pressure
477 transmitting media. Journal of Physics D-Applied Physics, 42(7).
478 Klug, D.D., Rousseau, R., Uehara, K., Bernasconi, M., Le Page, Y., and Tse, J.S. (2001) Ab initio
479 molecular dynamics study of the pressure-induced phase transformations in cristobalite.
480 Physical Review B, 63(10).
481 Kruger, M.B., and Jeanloz, R. (1990) Memory Glass - an Amorphous Material Formed from $AlPO_4$.
482 Science, 249(4969), 647-649.
483 Larson, A.C., and Dreele, R.B.V. (2000) GSAS: General structure analysis system. Los Alamos
484 National Laboratory Report LAUR, 86.
485 Liang, Y., Miranda, C.R., and Scandolo, S. (2007) Tuning oxygen packing in silica by
486 nonhydrostatic pressure. Physical Review Letters, 99(21), 215504-1.
487 Mao, H.K., Xu, J., and Bell, P.M. (1986) Calibration of the Ruby Pressure Gauge to 800-Kbar under
488 Quasi-Hydrostatic Conditions. Journal of Geophysical Research-Solid Earth and Planets,
489 91(B5), 4673-4676.
490 Ming, L.C., Nakamoto, Y., Endo, S., Chio, C.H., and Sharma, S.K. (2007) Phase transformations of
491 α-cristobalite $GaPO_4$ at pressures up to 52 GPa. Journal of Physics: Condensed Matter, 19,
492 425202.

Morris, J.H., Perkins, P.G., Rose, A.E.A., and Smith, W.E. (1977) Chemistry and Binding Properties of Aluminum Phosphates. Chemical Society Reviews, 6(2), 173-194.

Murashov, V.V., Dubrovinsky, L.S., Tse, J.S., and Lepage, Y. (1995) The pressure induced phase transition of the α cristobalite form of $CaPO_4$. Journal of Physics: Condensed Matter, 7, 8279.

Nicola, J.H., Scott, J.F., and Ng, H.N. (1978) Raman study of α-β cristobalite phase transition in $AlPO_4$. Physical Review B, 18, 1972-1976.

Olijnyk, H. (1990) High pressure x-ray diffraction studies on solid N2 upto 43.9 GPa. J. Chem. Phys, 93, 8968.

Palmer, D.C., and Finger, L.W. (1994) Pressure-Induced Phase-Transition in Cristobalite - an X-Ray-Powder Diffraction Study to 4.4 GPa. American Mineralogist, 79(1-2), 1-8.

Palmer, D.C., Hemley, R.J., and Prewitt, C.T. (1994) Raman-Spectroscopic Study of High-Pressure Phase-Transitions in Cristobalite. Physics and Chemistry of Minerals, 21(8), 481-488.

Pasternak, M.P., Rozenberg, G.K., Milner, A.P., Amanowicz, M., Zhou, T., Schwarz, U., Syassen, K., Taylor, R.D., Hanfland, M., and Brister, K. (1997) Pressure-Induced Concurrent Transformation to an Amorphous and Crystalline Phase in Berlinite-Type $FePO_4$. Physical Review Letters, 79, 4409-4412.

Pellicer-Porres, J., Saitta, A.M., Polian, A., Itie, J.P., and Hanfland, M. (2007) Six-fold-coordinated phosphorus by oxygen in AIPO(4) quartz homeotype under high pressure. Nature Materials, 6(9), 698-702.

Pitak, Y.N., and Churilova, Y.V. (2004) The Effect of Aluminum Phosphate Binder on the Crystallization of Mullite-Silica Fibers. Refr. and Ind. Cera., 45, 275-276.

Poswal, H.K., and Sharma, S.M. (2011) First principles investigations on cristobalite-$AlPO_4$. Manuscript under preparation.

Ramaniah, L.M., Sharma, S.M., Kunc, K., Garg, N., and Laghate, M. (2003) First-principles determination of the relative stability of the alpha and Cmcm structures of $AlPO_4$. Physical Review B, 68, 014119,1-7.

Robeson, J.L., Winters, R.R., and Hammack, W.S. (1994) Pressure induced transformations of the low cristobalite phase of $GaPO_4$. Physical Review Letters, 73, 1644-1647.

Rokita, M., Handke, M., and Monzgawa, W. (2000) The $AIPO_4$ polymorphs structure in the light of Raman and IR spectroscopy studies. Journal of Molecular Structure, 555, 251.

Sharma, S.M., Garg, N., and Sikka, S.K. (2000) High-pressure x-ray-diffraction study of alpha-$AlPO_4$. Physical Review B, 62(13), 8824-8827.

Shirley, R. (2004) Crysfire.

Smith, W., Leslie, M., and Forester, T.R. (2003) Computer code DL_POLY_2.14 (CCLRC,Daresbury laboratory, Daresbury, England).

Tse, J.S., and Klug, D.D. (1991) The Structure and Dynamics of Silica Polymorphs Using a 2-Body Effective Potential Model. Journal of Chemical Physics, 95(12), 9176-9185.

Tsuchida, Y., and Yagi, T. (1989) A New, Post-Stishovite High-Pressure Polymorph of Silica. Nature, 340(6230), 217-220.

Tsuneyuki, S., Matsui, Y., Aoki, H., and Tsukada, T. (1989) New pressure-induced structural transformations in silica obtained by computer simulation. Nature, 339, 209.

Tsuneyuki, S., Tsukada, M., Aoki, H., and Matsui, Y. (1988) First-Principles Interatomic Potential of Silica Applied to Molecular Dynamics. Physical Review Letters, 61(7), 869.

van Beest, B.W.H., Kramer, G.J., and Vansanten, R.A. (1990) Force-Fields for Silicas and Aluminophosphates Based on Abinitio Calculations. Physical Review Letters, 64(16), 1955-1958.